**HIGH ACCURACY EQUATIONS OF STATE FOR PLANETARY COLLISION MODELING.** R. G. Kraus[1], D. C. Swift[2], D. G. Hicks[2], and S. T. Stewart[1], [1]Harvard University (20 Oxford St. Cambridge, MA 02138, rkraus@fas.harvard.edu), [2]Lawrence Livermore National Laboratory (7000 East Ave, Livermore, CA).

**Introduction:** Planetary collisions generate shock pressures that can melt and vaporize large amounts of material. Unanswered questions in the growth and evolution of planets have progressed to the point where accurately determining how much melt and vapor is produced and the overall thermal history during a collision have become necessary. To make these predictions, accurate equations of state (EOS) must be implemented into shock physics codes. Here, we present empirically-constrained wide-ranging multi-phase equations of state for MgO and $SiO_2$.

The EOS of realistic planetary mantle compositions are well known over some, generally small, range of phase space due to experimental limitations. However, impact events sample a tremendously wide range of the phase diagram, from 100's of GPa and 10's of thousands of Kelvin to post-shock states passing through the liquid-vapor region. Researchers at facilities like the Z-machine at Sandia National Lab [1] and the Omega laser at the Univeristy of Rochester [2] are now making high-quality EOS measurements on mantle oxides over the entire range of pressures and temperatures accessed during planetary collisions. With these new data, we are developing accurate EOS models that can be easily implemented into collision models as tabulated EOS. As end member phases, MgO and $SiO_2$ are of particular interest to understand first.

**Generalized EOS model for Oxides:** Hydrocode calculations only require the pressure as a function of density and internal energy. However, the temperature and entropy terms in the free energy are required to determine the phase diagram at finite temperatures. As material phase can dramatically effect the post-impact evolution, we pay particular attention to the temperature and entropy within the EOS models.

Our model equations of state are based upon Helmholtz free energy surfaces for individual phases. All thermodynamic parameters can then be derived from appropriate derivatives. The multiphase EOS is constructed by minimizing the Gibbs free energy at a given pressure and temperature. We model each free energy surface as the sum of cold curve $E_c$, a thermal contribution from the nuclei $F_{th}$, and an electronic contribution $F_e$.

**Solid Equation of State:** Where available, cold compression curves of solid phases are taken from experimental data. If no experimental data is available, as at ultra-high pressures, results from first principles calculations are used to fit the cold curve.

The thermal contribution to the free energy of solids is modeled in the quasi-harmonic approximation with an anharmonic perturbation. Although used in many EOS models, the Debye model does not accurately model the heat capacity, and hence entropy, of most oxides. Consequently, we use the Kieffer model [3], which includes high-frequency optic modes, for the vibrational density of states of the solid phases. The Grüneisen parameter, which describes the volume dependence of the vibrational density of states, is fitted to match the solid Hugoniot data. The anharmonic perturbation to the free energy is constrained by high-temperature vibrational spectroscopy and shock temperature measurements. For non-iron bearing minerals, the electronic contribution is generally negligible in the solid.

**Fluid Equation of State:** Currently, a Vinet compression curve is used to model the compressed cold curve of the fluid phase. The three parameters are constrained by the fluid Hugoniot. A Mie-type cold curve has been shown to be adequate for modeling the expanded region [4, 5], however, future liquid-vapor curve measurements will be used to determine the universality of the Mie-type potential for mantle oxides.

The thermal contribution to the free energy of the liquid is based on an Einstein oscillator model. However, we include molecular dissociation in the high-density fluid by defining a partition function for the molecules and minimizing the free energy. This method is similar to that described in [4] for the gas phase. Again, the Gruneisen parameter is used to match the thermal pressure on the Hugoniot.

The electronic contribution to the free energy of the fluid phase at 100's of GPa is non-negligible [2]. Our current treatment is a two term polynomial function in temperature that allows us to match the shock temperature and entropy. The electronic pressure is currently not included and is compensated for by the thermal Grüneisen parameter.

**EOS for $SiO_2$:** The EOS in development for $SiO_2$ (Fig. 1) includes $\alpha$-quartz or silica glass as the starting phase, stishovite as the high pressure phase, and a fluid phase that will include a robust liquid-vapor curve. Except at the lowest pressures where strength dominates, the model Hugoniots of all the phases are in excellent agreement with experimental pressure, density, and temperature data. The entropy along the model Hugoniot also matches a recent calculation of the entropy along the quartz Hugoniot [5].

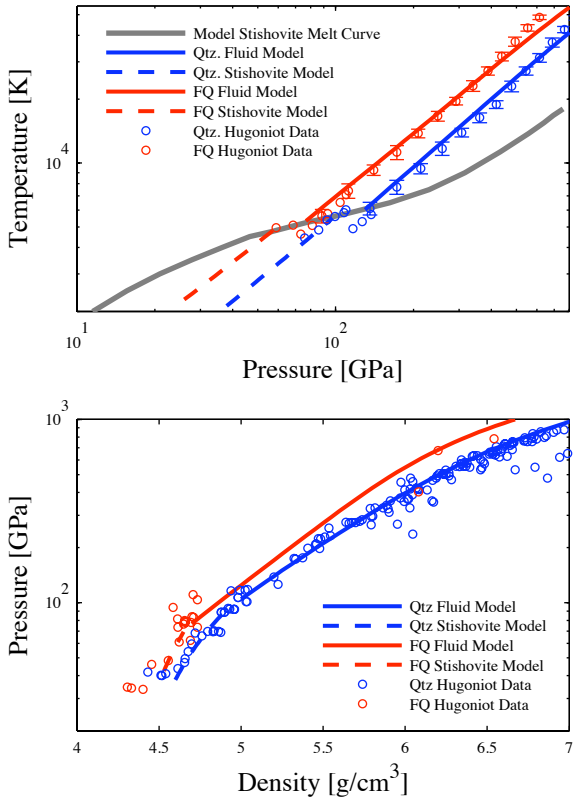


Figure 1: (Top) Pressure-temperature phase diagram with model Hugoniot for fused quartz (red) and α-quartz (blue) in the stishovite phase (dashed) and fluid phase (solid). Shock temperature data are from [2, 6]. (Bottom) Pressure-density hugoniot data for fused quartz and α –quartz in the solid and fluid phase. Quartz fluid Hugoniot data is compiled in [1]. Hugoniot data in the stishovite phase is from [6, 7].

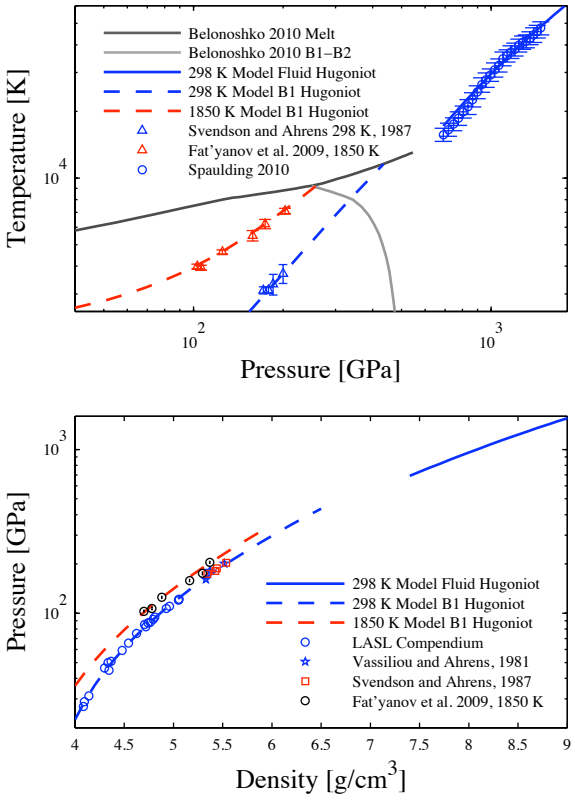


Figure 2: (Top) Pressure-temperature phase diagram from [8] with model Hugoniot for room temperature MgO [9, 10] (blue) and MgO preheated to 1850 K [11](red) in the B1 phase (dashed) and fluid phase (solid). (Bottom) Pressure-density Hugoniot data [9, 11-13] and model for MgO in the B1 and fluid phases. The B1 and fluid Hugoniots are in excellent agreement with recent shock wave experiments performed at the Sandia Z-machine.

**EOS for MgO:** The phase diagram of MgO is relatively simple, though difficult to access experimentally as the stability field of the rocksalt (B1) structure is so large. The EOS in development for MgO (Fig. 2) includes the B1 and fluid phase. The melt boundary will be constructed once the B2 phase is added.

**Experiments in Progress and Planned:** The temperature on the liquid-vapor curve of silica has been measured [5]. Experiments to measure the temperature and density on the liquid-vapor curve of MgO are currently being performed on the Z-machine at Sandia. Future experiments on the fluid Hugoniot and liquid-vapor curve of Fe, $MgSiO_3$ and $Mg_2SiO_4$ are planned for late 2012 and 2013 at the Z-machine.

**Model Improvements and Future Directions:** Initial attempts at modeling the liquid-vapor curve of MgO using the formalism of M-ANEOS [4] proved difficult. With more data on the liquid-vapor curve of oxides we will settle on a formalism for the free energy in the liquid-vapor region of the phase diagram.

The heat capacity of the nuclei in the fluid model currently extrapolates to a value of $3k_b$/atom at high T, when the limit should be $1.5k_b$/atom. A density and temperature dependent electronic free energy term will soon be included that utilizes shock reflectivity measurements to constrain the density dependence.

The physics models being developed for the mantle endmembers, $SiO_2$ and MgO, will be used to develop multi-phase equations of state for dominant mantle compositions, once more data are available.

**References:** [1] Knudson, M.D. and M.P. Desjarlais (2009) *PRL* **103**(22), 225501. [2] Hicks, D.G., et al. (2006) *PRL* **97**(2), 025502. [3] Kieffer, S.W. (1979) *Rev. Geophys.* **17**(1), 1-19. [4] Melosh, H.J. (2007) *MAPS* **42**(12), 2079-2098. [5] Kraus, R.G., et al. (2012) *in prep. for JGR-Planets*. [6] Lyzenga, G.A., T.J. Ahrens, and A.C. Mitchell (1983) *JGR* **88**(NB3), 2431-2444. [7] Wackerle, J. (1962) *J. Appl. Phys.* **33**(3). [8] Belonoshko, A.B., et al. (2010) *Phys. Rev. B* **81**, 054110. [9] Svendson, B. and T.J. Ahrens (1987) *Geophys. J. R. astr. Soc.* **91**, 667-691. [10] Spaulding, D.K. (2011), UC Berkeley. [11] Fat'yanov, O.V., P.D. Asimow, and T.J. Ahrens (2009) *SCCM-2009*, AIP. 855-858. [12] Vassilious, M.S. and T.J. Ahrens (1981) *GRL* **8**(7), 729-732. [13] Marsh, S.P., ed. *LASL Compendium*. 1980, University of California Press.

**Acknowledgement:** RGK acknowledges the NNSA SSGF program.